# SPECIAL TRAITS OF THE MILLIMETER WAVE RELATIVISTIC MAGNETRON

*S.A. Berdin, K.V. Chizhov, N.P. Gadetski, V.G. Korenev, A.N. Lebedenko, M.I. Marchenko, I.I. Magda, O.G. Melezhik, V.G. Sinitsin, V.A. Soshenko*
*National Science Center "Kharkov Institute of Physics and Technology", Kharkov, Ukraine*
*E-mail: magda@kipt.kharkov.ua*

A 8 mm band relativistic magnetron is investigated experimentally and by means of numerical simulation. The physical effects are analyzed which influence negatively the r.f. generation. The processes capable of reducing effectiveness of the generation and duration of the generated pulse include forward and backward axial flows of electrons, and intense electric fields – the generated microwaves and the fields owing to the space charge.

PACS: 52.80.Pi

## INTRODUCTION

The paper presents results in the sequel of our studies [1, 2] of the millimeter wave relativistic magnetron (RM). A number of physical phenomena are considered which can negatively affect the operation of a RM, specifically the 'spurious' electron flows in the electrodynamic structure (EDS), not contributing directly to the r.f. generation, and the electric fields of high intensity in the anode-cathode gap (both the generated r.f. field and that of the space charge) which apparently randomize the **E×B** drift motion of electrons, thus violating the wave-particle velocity synchronism necessary for the generation.

## 1. MAGNETRON STRUCTURE

The diode system of a millimeter wave RM is expected to meet some mutually contradicting conditions. On the one hand, it seems desirable to increase the gap size $d_{CA}$, such that appearance and extension of the near-electrode plasma should not affect excitation of the EDS eigenmodes [3]. On the other hand, the drifting electron flow should move closer to the EDS resonators in order to maximize the particle-field interaction in the generated microwaves (hence, $d_{CA} < \lambda/2$). With this in mind, we have created a few versions of the millimeter wave relativistic magnetron with coaxial extraction. The latest version of the coaxial structure is shown schematically in Fig. 1. It allows quick replacement of the cathode and basic units of the EDS, as well as of the microwave extraction unit.

The high voltage input pulse ($U_0$=100…350 kV, $t_P$=35…40 ns) is fed from a dual pulse-forming line with the output impedance 16 Ohm which is connected to the coaxial vacuum diode *1* (see Fig. 1). The multicavity resonant EDS of the magnetron, incorporated in the anode block *8* ends with an axial extraction unit for the microwave energy, coupled to a conic horn *9*. The EDS is placed inside an oversized circular vacuum waveguide *10* (made of a stainless steel pipe, diameter 80 mm and $L$=600 mm), provided with a radiotransparent window at the end face. At the same time, the waveguide *10* serves as a current collector and an electrode for return currents from the anode block and the collector electrode. The removable cylindrical cathode *7* (made of stainless steel, $d_C$=12…16 mm) is fixed to a long holder *6* (stainless steel, $d_H$=12 mm). The cathode-anode gap ($d_{CA}$=3 to 8 mm) is specified by the diameter of the replaceable cathode.

To measure axial currents and further estimate the anode and the collector current magnitudes, two net current monitors *3* and *4* (Rogowski coils) are placed to the left and to the right of the EDS unit.

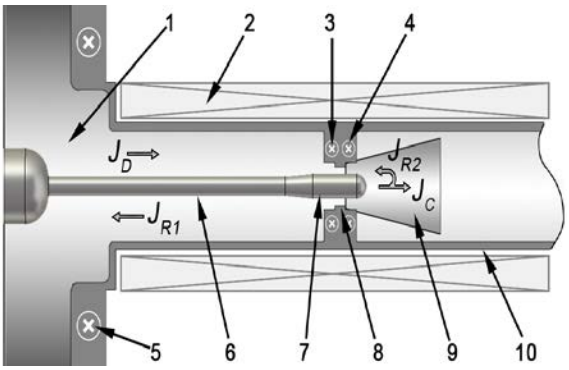


*Fig. 1. Schematic view of the RM: 1 – vacuum diode; 2 – impulse solenoid; 3, 4 and 5 – current monitors; 6 – cathode holder; 7 – cathode; 8 – anode block (ESD); 9 – horn; 10 – oversized waveguide*

The outer surface of the waveguide *10* accommodates the impulse solenoid *2* that serves to create a focusing magnetic field of induction up to 0.8 T. The edge fields of the solenoid have been calculated so as to minimize the damage of surfaces of the vacuum diode's dielectric insulator and the extracting window impacted by the electron flows emitted by different parts of the cathode holder *6*.

## 2. PERFORMANCE OF RM48

The results of experiments (and of theoretical analyses) showed no qualitative distinctions between EDSs with different numbers $N$ of resonators (i.e., $N$=32, 40 or 48), therefore we will quote below only the data for $N$=48.

The geometries of the EDS and the conical microwave extracting horn had been pre-optimized within a numerical 3D model that employed a particle-in-cell (PIC) simulation technique. The same simulator was used to study the particle and field dynamics in the magnetron, under the conditions of either fixed or electric field dependent (explosive) emission from the cathode.

### 2.1. EIGENMODES OF THE EDS

The eigenfrequencies of a 'cold' EDS are given by a dispersion relation which has been derived here for a coaxial structure of a finite length along the $z$-axis. With

the assumption that the dependence upon $z$ is absent ($\frac{\partial}{\partial z} = 0$, the 2D case) the general relation splits into two independent equations for TE and TM modes, respectively, each of the form that was first derived back in 1940s [4]. A mathematically rigorous derivation and analysis of the 2D equation for TE modes were later suggested in paper [5]. Shown in Fig. 2,a are dispersion curves of free microwave oscillations in a 'cold' EDS of the RM48, computed within the 2D approximation for two spatial harmonics ($m$=0 and $m$=1). The points where these curves intersect with the straight lines $2\pi f = kv_D$, representing the dispersion law of an electron beam that moves at the drift velocity $v_D$ through crossed **E** and **B** fields, determine possible operating frequencies of the device. As can be seen in the Figure, beam velocities $v_D$ about (0.1…0.3)$c$ suggest a possibility of driving oscillations similar to the $\pi$-mode, at four frequencies from the range (37.5 to 43 GHz) of the fundamental spatial harmonic, and close to the $\pi/2$-mode at three higher frequencies within the first spatial harmonic.

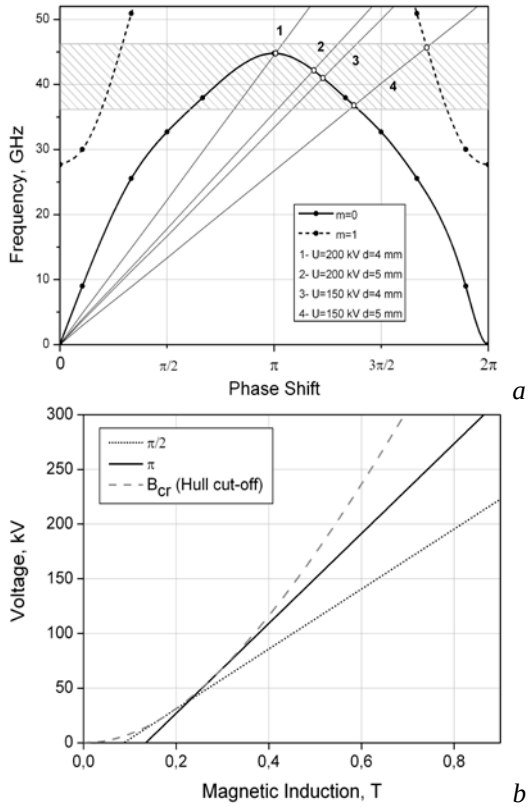


*Fig. 2. The dispersion diagram (a) and operational regimes (Hartrey-Buneman diagram) (b) for the RM48, $d_{CA}$=5 mm*

The results are in agreement with the computed operation regimes of the RM48 shown in Fig. 2,b. The operation diagram is based on Hull's cut-off condition for the anode current, and resonant excitation of the EDS by a Brillouin drift flow in crossed $\mathbf{E_0}$ and $\mathbf{B_0}$ fields, as obtained with account of relativistic corrections, following paper [6].

### 2.2. RESULTS OF EXPERIMENTS AND 3-D SIMULATIONS

The generation of microwaves was observed in the RM48 in a broad range of magnetic fields, $B_0$=0.35 to 0.8 T and applied voltages, $U_0$=100…300 kV. The generated frequencies lay within 37…43 GHz. The operation parameters (namely, frequencies, oscillation modes and excitation conditions) were in a fair agreement with the computed results that follow from the dispersion relation (see Fig. 2,a) and the operation diagram (see Fig. 2,b), as well as from numerical simulations of an operating RM48. The simulations corroborated excitation of oscillations close to the $\pi$-mode and less frequently, to $\pi/2$-mode for $m$=0, -1 spatial harmonics.

Fig. 3 illustrates the r.f. electric field distribution near the surface of the EDS and the millimeter-band spectrum obtained for a typical structure and driving conditions of the RM48, namely $d_A$=22 mm, $d_{CA}$=3.5 mm, $L_A$=6 mm, applied voltage at the cathode -150 kV and magnetic field induction 0.43 T. As seen in the left (*a*) part of the Fig. 3, the r.f electric field component demonstrates a spatial pattern very close to the distribution in the $\pi$-mode. The spectrum estimated for the output horn (see Fig. 3,b) also corresponds to the analytical prediction for this mode (i.e. a frequency line about 37 to 41 GHz).

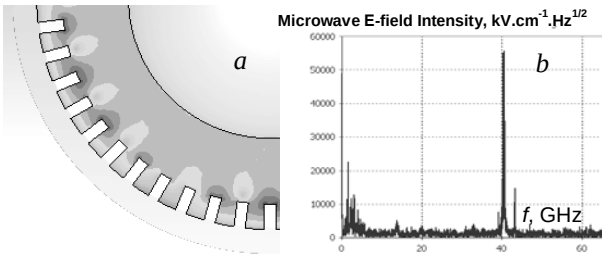


*Fig. 3. Electric field distribution near the resonators (a), and spectral density of the radiated electric field in the horn (b) (J=0.5 kA, $B_0$=0.43 T, and $d_{CA}$=3.5 mm)*

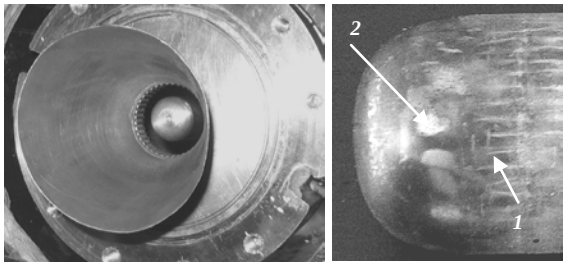


*Fig. 4. General view of the anode block, with the microwave extraction horn and casing of the Rogowski coil (left panel), and structured traces of electric discharges on the cathode (right panel)*

Fig. 4 shows traces left by microwave discharges on the cathode of the RM48. It seems likely that the longitudinal strips *1* on the cathode result from small-scale discharges controlled by the local spatial structure of the EDS, while the spots *2* correspond to larger scale discharges occurring in concentration areas of the E-field, near edges of the EDS resonators. The disposition of the microwave breakdown spots, namely at every other period of the EDS structure that was manifested in the majority of cases of generation in the experiment, is evidence for oscillations of the $\pi$ mode.

Fig. 5 presents measured intensities $I_\mu$ of the microwave signal in dependence on strengths of the electric field in the cathode-anode gap and the external magnetic field, $I_\mu(E_0,B_0)$. The three groups of points in the Figure correspond to electric field strengths $E_0$ calculated for

several gap widths (3, 4, and 5 mm) and different applied voltages, 110 to 200 kV. The three groups are well separated along the field strength axis, $E_0$, while within the groups the measured points demonstrate similar $I_\mu(E_0)$ and $I_\mu(B_0)$ dependences. As can be seen, each of the groups contains an area of sharp $I_\mu(E_0, B_0)$ variations, with the value dropping off toward smaller $E_0$ and $B_0$ (Hull's cut-off). Another area corresponds to a maximum generated intensity, and yet another to a moderate fall-off at high values of $E_0$ and $B_0$.

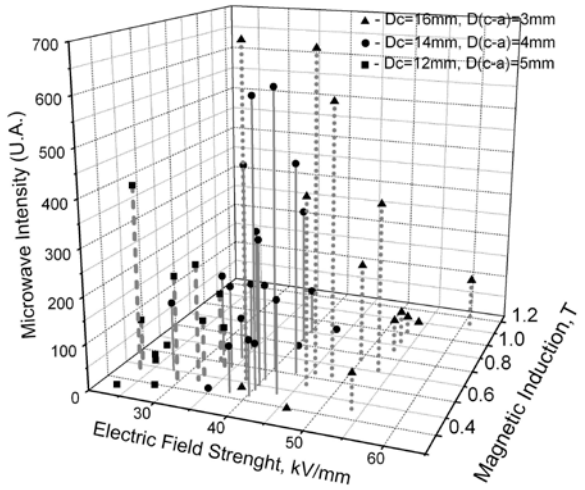


*Fig. 5. Radiated field intensities from the RM48 for a variety of $E_0$ and $B_0$*

## 3. FACTORS TO UPSET GENERATION

The experiments have shown that the conditions enabling microwave generation were fulfilled only over a part of the full current's pulse duration. The r.f. pulse was, in practically all operational regimes, of a much shorter length than the driving impulse. The duration could vary between 2 ns and 7 ns depending on the operating conditions (Fig. 6,a). Also, the r.f. emission was characterized by a noticeable variability of parameters and low efficiency in terms of power, $P$. The electron efficiency of the RM estimated as the ratio $P_\mu/(U_0 I_0)$ never exceeded 1%.

Apparently, we have faced some impeding factors during our experiments that are capable of deteriorating magnetron generation in a much tougher way than is typical for relativistic magnetrons of the X-band [3, 7]. Appealing to the knowledge of destructive processes in millimeter wave relativistic devices of O-type [8], we can indicate probable unfavorable effects for the RM as well, namely plasma formation along surfaces of the device electrodes in static E-fields; anode bombardment, and microwave breakdown.

In view of the characteristically short duration of the generation pulse in the RM48 ($t_\mu$=2 to 7 ns) the effect of cathode-anode gap filling with the plasma due to the static electric field cannot be significant. Indeed, the inter-electrode plasma flows manifest themselves after times about $t_{\text{diff}}$ corresponding to ambipolar diffusion in a magnetized diode. The diffusion rate normally is $v_{\text{diff}} \approx$ (10 to 20) mm/μs [3], hence for the 3 to 5 mm gaps representative of the experimental magnetrons ($N$=48) we obtain $t_{\text{diff}} \approx$150…500 ns, which is much longer than the r.f. generation times $t_\mu$ (once again, μ stands for 'microwave').

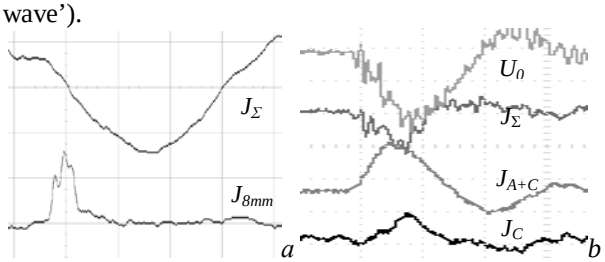


*Fig. 6. Net current waveform $J_\Sigma$ in current monitor 5 (cf. Fig. 1) and that of the λ= 8 mm signal in the RM, 10 ns/div (a). Voltage and current pulsed waveforms in monitors 5, 3, and 4, 25 ns/div (b)*

More effective, at a first glance, seem to be the plasma processes that develop along the EDS surface over lengths about the structure's spatial period (say, 2 mm as in our case). Then the plasma particles moving along magnetic lines of force have enough time to cover resonator lengths over $t_{\text{diff}}$ about tens of nanoseconds. The quickest among plasma formation processes is the electric breakdown between the resonators, owing to microwave fields. However, for the breakdown to occur it is necessary that the generated r.f. field should have increased to the critical discharge level. The threshold condition known for vacuum electronics devices is a voltage level of 10 to 20 MV/m [8], also dependent on the pulse duration. The familiar O-type devices generate millimeter wave pulses of duration 50 to 100 ns at power levels of a few hundred megawatts [9]. If in their case the pulse duration and intensity had been limited by r.f. breakdowns between the resonator electrodes, then the characteristic generation time $t_\mu$ in the magnetron should have been estimated as roughly of the same magnitude. Quite evidently, this is not so, and the limiting factors acting in the magnetron are tougher.

Another factor that can negatively affect the generated pulse intensity and duration in the RM is the existence of paraxial electron flows (moving both in the forward and back directions), whose presence is confirmed by the data of our measurements and 3D simulation of the current distribution about the EDS.

Similar to the test mockup, the 3D numerical model of the RM48 also involved several current monitors, placed in different parts of the coaxial structure (Fig. 7). The monitors allowed following the dynamics of the spatially separated electron flows. One appears in the diode block in the form of a drift current associated with the anode current $J_A$. Another one flows along the surface of the cathode holder, being a result of explosive emission from the cathode and the holder. Yet another flux of electrons, $J_C$, is emitted from the end face of the cathode and passes toward the collector (i.e., the output end of the oversized waveguide). When the magnitude of $J_C$ reaches a certain critical level, a virtual cathode appears in the space behind the cathode, giving rise to a reverse current flow $J_{R2}$. In the experimental set-up, the total magnetron current and the three electron flows are fixed by the current sensors *5*, *3* and *4* (see Fig. 1), respectively as $J_\Sigma = J_D$-$J_{R1}$; $J_{A+C}$, and $J_C$-$J_{R2}$, Fig. 6,b.

As is seen from the numerical model, the current $J_{R1}$ is formed on the surface of the cathode holder with some delay relative to the emission current $J_A$ depend-

ing on the explosive emission threshold. Similarly, the current $J_{R2}$ (if developed) shows a lag relative emission from the cathode's end face (current $J_C$).

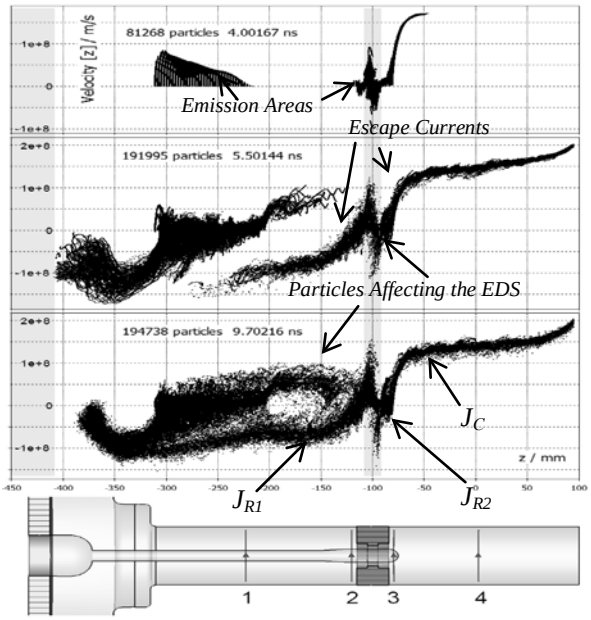


*Fig. 7. Dynamical axial distribution of the $v_Z$ velocity component for all particles in the RM and characteristic currents through the RM at moments 4.0, 5.5, and 9.7 ns*

Each of the electron flows formed in the RM is characterized by a spatial structure and variation dynamics of its own, which can be seen in the diagrams of fluxes with a given particle velocity. The essential features of these current flows are reflected in the distributions along the *z*-axis of the axial velocity $v_Z$ which are given in Fig. 7 for a number of consecutive time moments.

They are

- appearance of non-stationary secondary centers of explosive emission on the surface of the cathode holder;
- formation of particle flows streaming in both directions along the RM axis ('escape currents');
- slowing down of the particles and formation of a virtual cathode in the space behind the anode block at extreme magnitudes of the current $J_C$, accompanied by appearance of electrons with reversed velocities;
- intense sedimentation upon the electrodes of the particles that badly affect the EDS.

The particle flows are naturally divided into two groups, namely forward currents ($J_D$ and $J_C$), streaming toward the microwave extraction, and reverse currents ($J_{R1}$, $J_{R2}$) that flow toward the vacuum-diode interface. It should be noted that the spurious reverse currents $J_{R1}$ and $J_{R2}$ may be greater in magnitude than the anode current ($J_A \approx 50\ldots350$ A) by a factor of upon the electrodes ~$10^1$ to $10^2$. The dependences of these currents upon the magnetic induction $B_0$ as obtained in the experiments are shown in Fig. 8. The difference $J_\Sigma$-$J_{A+C}$ (dashed line in the Figure) gives an estimate for the reverse current $J_{R1}$ along the cathode holder, while the difference $J_{A+C}$–$J_C$ (solid line) represents the anode current $J_A$. As can be seen from the Figure, the spurious reverse currents are essentially suppressed when the magnetic induction is increased. Meanwhile, the noticeable reduction observed in the magnitude of the anode current suggests a necessity of concurrently increasing the applied voltage $U_0$.

The dependences shown by the data from current monitors (specifically, on the magnetic induction, accelerating electric field and explosive emission threshold) are confirmed by the 3D simulations (see Fig. 7). Four magnitudes of the induction (0.2 T; 0.35 T; 0.45 T, and 0.7 T) and two values of the emission threshold ($1\cdot10^7$ and $2\cdot10^7$ V/m) were taken for the modeling.

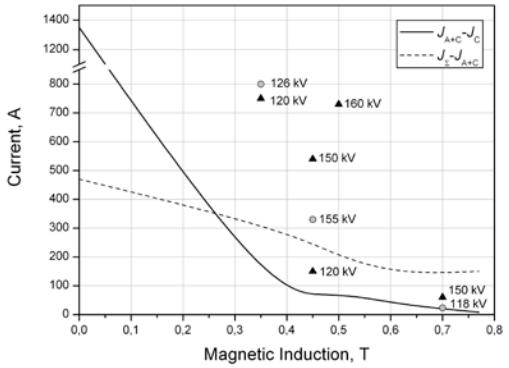


*Fig. 8. The reverse current $J_{R1}$ and anode current $J_A$ as functions of magnetic induction, with applied voltages $U_0$ ranging from 100 to 150 kV, for two assumptions on the threshold magnitude of the explosive emission field (▲,$E_{th}$ =$1\cdot10^7$ V/m and ○, $E_{th}$ =$2\cdot10^7$ V/m)*

The anode current estimates obtained within the numerical model for several voltages across the cathode-anode gap are given in Fig. 8 together with the measured values. The simulated anode current can be seen to depend essentially on the anode voltage, which was not as evident in the experiment.

Among the reasons randomizing the drift motion of resonant electrons in the RM, the destructive action of the generated r.f. fields and of the fields due to the space charge should be particularly noted. The field strengths may reach high enough values to become commensurate with the levels of the external (applied) $E_0$ and $B_0$ fields which provide for the drift motion of particles.

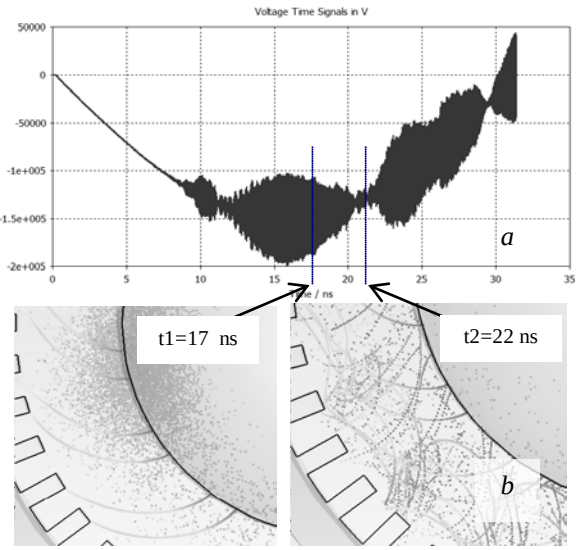


*Fig. 9. Signal from the voltage monitor in the interaction space (a), and spatial distributions of particles in the gap for different time moments (b)*

Fig. 9,b shows 2D projections of spatial particle distributions that were obtained in the 3D numerical model

for two positions (time moments) on the pulsed voltage waveform $U_0+U_\mu$ acting in the anode-cathode gap (see Fig. 9,a). The specific moments correspond to intense generation of microwaves ($t_1$=17 ns) and to quenching of the oscillations ($t_2$ = 22 ns). It is clearly seen in Fig. 9,b how the smooth trajectories, nearly tangent to the surface of the EDS, that are typical of the former case (i.e., pronounced r.f. generation) are replaced in the latter by kinked curves, often with an inverted sign of curvature. The effect might be evidence for a change in sign of the local component of the net field $E_0+E_\mu$ (or, maybe $B_0+B_\mu$) owing to greatly increased r.f. field intensity. The appearance of similar alternating areas (they should be localized in microwave field crests of a proper sign) shall inevitably result in chaotization of the particle flow, and hence in a sharply diminished efficiency of the field-particle interaction.

Numerical simulation of similar 'self-limited' modes of generation reveals possibilities for appearance of repetitive relaxation oscillations of periods 2 to 5 ns, and the corresponding randomization of the generated spectra. As an alternative, optimal generation regimes also exist (Fig. 10). They are characterized by a stable generation of millimeter waves of noticeably greater intensity. Thus, at $U_0$=150 kV; $B_0$=0.43 T, and $d_{CA}$=3.5 mm the current emitted from the cathode stayed at an optimum level close to 1 kA.

Concerning the space-charge fields developing in the interaction space, it seems that their effects are not as clearly localized in the vicinity of the anode surface, in particular because of the small width of the anode-cathode gap. Meanwhile, the relativistic magnetron is a device very suitable for realizing space charge-limited current regimes. It is then quite understandable that any deviation from an equilibrium density distribution (e.g., bunching of the particles) may result in a global deterioration of the resonant drifting flow (Brillouin beam) and suppression of the generation process.

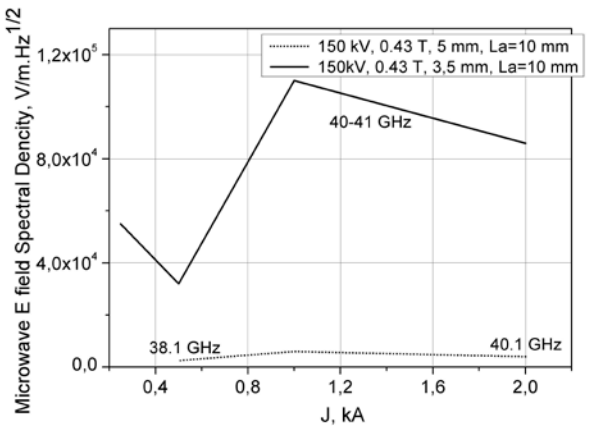


*Fig. 10. Intensity of microwave generation in the RM as a function of the current emitted from the diode (two sizes of the anode-cathode gap)*

In conclusion, yet another reason will be noted which impedes efficient generation of millimeter wavelengths in RMs. It is the 'miniature' size of the anode-cathode gap and of the whole structure. With characteristic applied voltages of hundreds of kilovolts and gap sizes of a few millimeters, electric field strengths in the gap may be as high as $10^2$ MV/m. These lead to a quick breakdown, thus limiting the duration of r.f. generation to units of nanoseconds.

## CONCLUSIONS

The experimental and numerical analyses of the RM, focused on a study of current distributions in and around the electrodynamic structure, have revealed a set of effects, negatively influencing the efficiency of microwave generation and reducing its duration. Before all, this is the pre-axial transfer of particles (both in the forward and back directions) tending to randomize the resonant drift flows of particles in the interaction space. A very special effect is the deterioration of drift particle trajectories under the action of intense *E*- and *B*-fields due to the microwave generation and to space charge development. The latter are kind of an attribute of the millimeter wave RM, owing to its 'critical' currents and current limitation mechanisms. Other effects include the known plasma forming phenomena which are also manifested stronger in small-sized EDSs of the millimeter wave devices.

## REFERENCES


1. I.I. Magda, S.A. Berdin, N.P. Gadetsky, et al. Relativistic Magnetron of Millimeter Waveband // *18-th Int'l Crimean Conference 'Microwave and Telecommunication Technologies,'* 2008, Sevastopol, Crimea, Ukraine, p. 637-639.
2. I.I. Magda, N.P. Gadetski, E.I. Kravtsova, et al. Relativistic Magnetron of 8 mm Waveband // *Problems of Atomic Science and Technology. Series "Plasma Electronics and New Methods of Acceleration"*. 2008, № 4, p. 18-20.
3. J. Benford. Pulse Shortening in Magnetrons // *Proc. of EUROEM'94 International Symp*. Bordeaux, France, 1994, v. 2, p. 170-174.
4. J.B. Collins. *Microwave Magnetrons.* McGraw-Hill, New York, 1948.
5. Y.A. Prokopchuk and V.G. Sologub. Eigen-oscillations of a Magnetron-type Resonator Structure // *Radiotechnika. The Inter-departmental (Ukrainian SSR) Collection of Research Papers,* 1969, Kharkov, iss. 10, p. 216-221.
6. O. Buneman. *Cross-Field Microwave Devices* / Ed. by E. Okress. New York, 1961, v. 1, p. 209.
7. J. Benford and J.A. Swegle. *High power microwaves*. Artech House, Inc., Boston, London. 1992, p. 149.
8. F.J. Agee. Evolution of Pulse Shortening Research in Narrow Band, High Power Microwave Devices // *IEEE Trans. Plasma Sci.* 1998, v. 26, p. 235.
9. S.P. Bugaev, V.I. Korovin, A.I. Klimov, et al. Physical Processes in Multiwave Cherenkov Oscillators // *Relativistic Microwave Electronics*. Gorky: Appl. Phys. Inst., Acad. Sci. USSR. 1988, v. 5, p.78-100.


*Article received 28.02.2014*

**ОСОБЕННОСТИ РЕЛЯТИВИСТСКОГО МАГНЕТРОНА МИЛЛИМЕТРОВОГО ДИАПАЗОНА**

***С.А. Бердин, К.В. Чижов, Н.П. Гадецкий, В.Г. Коренев, А.Н. Лебеденко, М.И. Марченко, И.И. Магда, О.Г. Мележик, В.Г. Синицын, В.А. Сошенко***

Экспериментально и методами численного моделирования проведено исследование релятивистского магнетрона 8-миллиметрового диапазона и анализ факторов, оказывающих негативное действие на генерацию. Отмечается, что к процессам, уменьшающим эффективность и длительность импульса генерации, относятся прямые и обратные осевые потоки электронов, интенсивные собственные ВЧ-поля и поля объемного заряда.

**ОСОБЛИВОСТІ РЕЛЯТИВІСТСЬКОГО МАГНЕТРОНА В МІЛІМЕТРОВОМУ ДІАПАЗОНІ ХВИЛЬ**

***С.А. Бердін, К.В. Чижов, Н.П. Гадецький, В.Г. Коренєв, О.М. Лебеденко, М.І. Марченко, І.І. Магда, О.Г. Мележик, В.Г. Сініцин, В.А. Сошенко***

Експериментально й методами чисельного моделювання досліджено релятивістський магнетрон діапазону 8 мм та проведено аналіз факторів, що негативно впливають на генерацію. Визначено, що до процесів, котрі зменшують ефективність та тривалість імпульсу генерації, відносяться прямі та зворотні осьові потоки електронів, інтенсивні власні ВЧ-поля і поля об’ємного заряду.